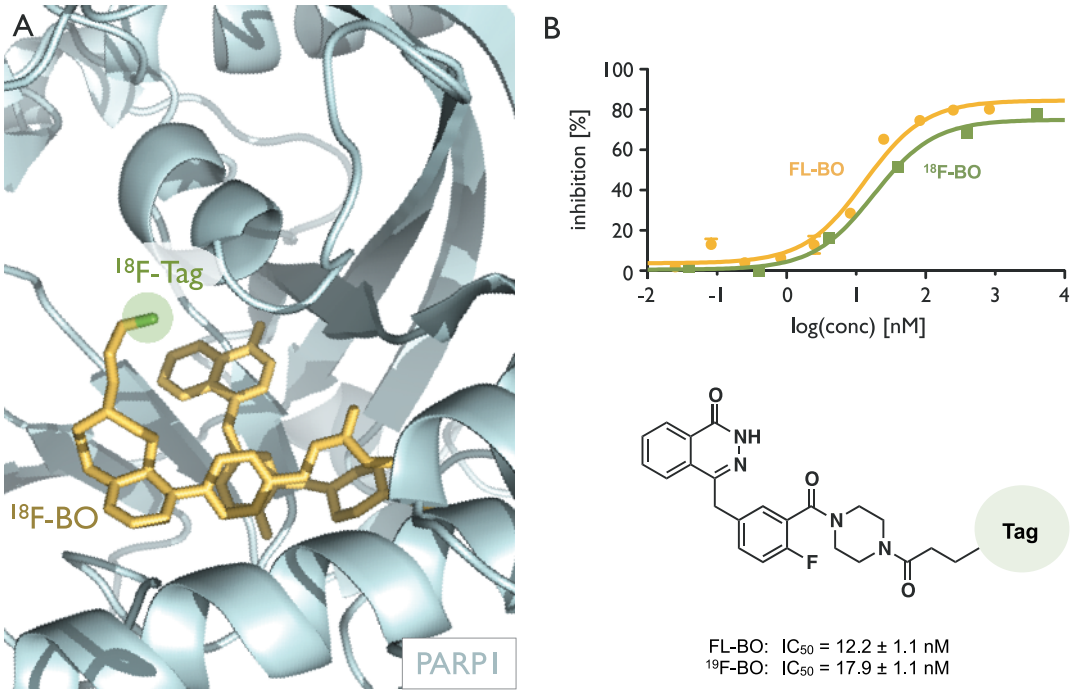


**Figure W1.** $^{18}$F-BO and FL-BO. (A) Binding model depicting $^{18}$F-BO and PARP-1, with the 2*H*-phthalazin-1-one binding to the catalytically active site on PARP-1. (B) $IC_{50}$ curves and values for $^{18}$F-BO and FL-BO (from Keliher et al. [8]).

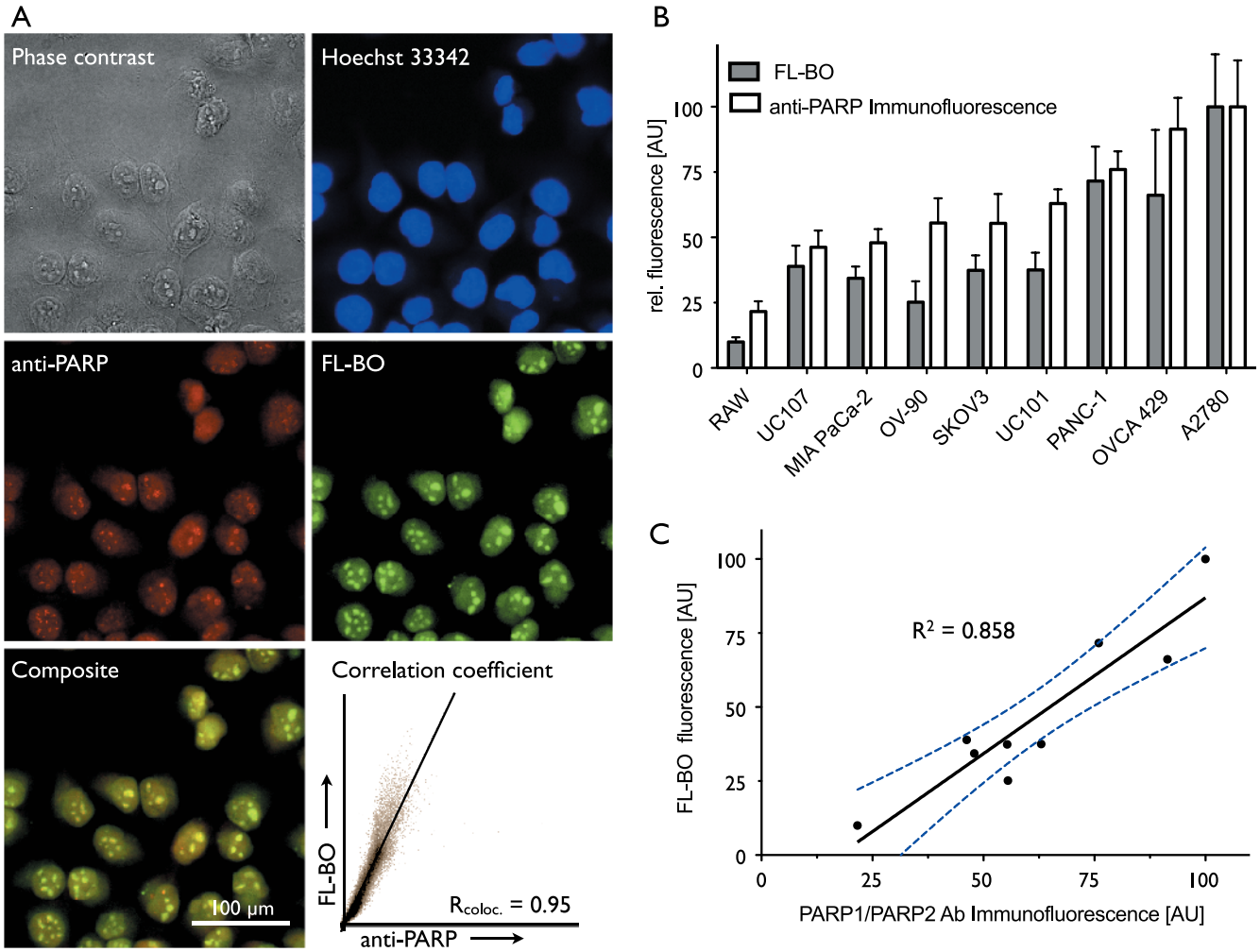


**Figure W2.** Correlation of cellular FL-BO uptake and relative PARP expression. (A) In PANC-1 cells, there was an excellent correlation between intracellular FL-BO distribution and PARP-1/2 expression: phase contrast (grayscale), Hoechst 33342 (blue), anti-PARP (red), FL-BO (green), composite image of anti-PARP and FL-BO, and Pearson correlation coefficient of anti-PARP and FL-BO. (B) Column representation of FL-BO uptake and anti-PARP immunofluorescence in different cell lines. (C) Correlation of FL-BO uptake and anti–PARP-1/2 immunofluorescence (blue line indicates the 95% confidence band).

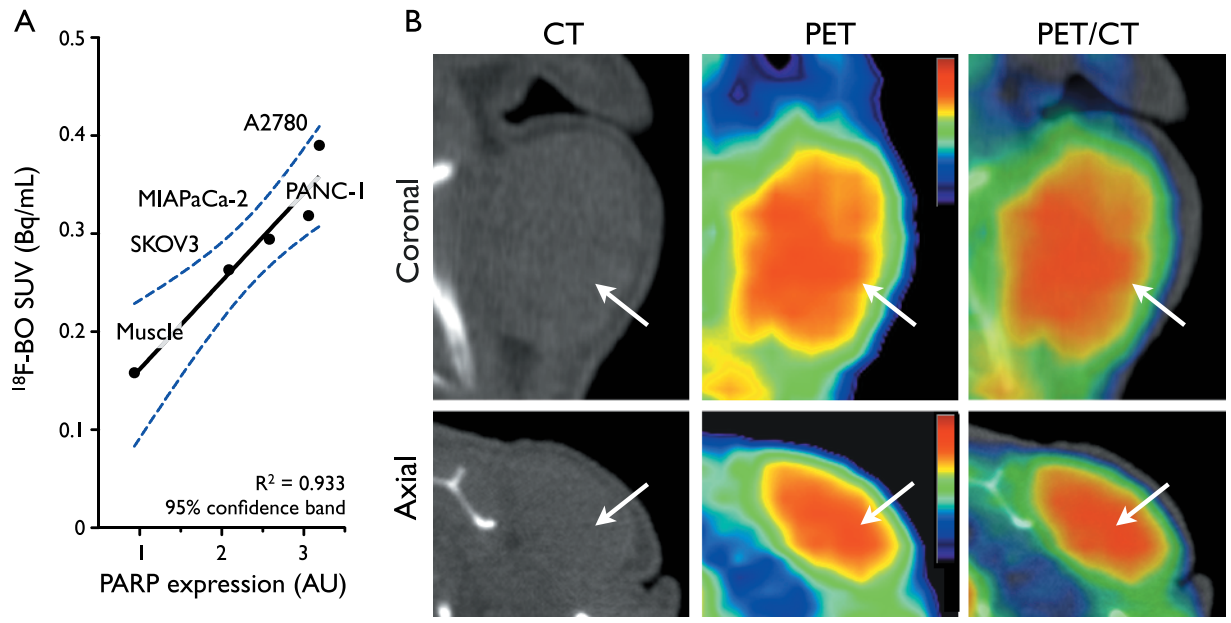


**Figure W3.** Correlation of PARP expression and $^{18}$F-BO uptake in tumor tissue. (A) correlation of uptake and PARP expression in four different ovarian and pancreatic tumor types as determined by immunoblotting. (B) coronal and axial CT and PET scans of a representative A2780 tumor implanted in the shoulder of a mouse.